Robust Pulmonary Lobe Segmentation Against Incomplete Fissures

Suicheng Gu[a], Qingfeng Zheng[b], Jill Siegfried[c], Jiantao Pu[ad*]

[a]Department of Radiology, University of Pittsburgh, 3362 Fifth Avenue, Pittsburgh, PA 15213

[b]Thoracic Surgery II, Key laboratory of Carcinogenesis and Translational Research (Ministry of Education), Peking University School of Oncology, Beijing Cancer Hospital & Institute, Beijing, 100142

[c]University of Pittsburgh Cancer Institute, 3362 Fifth Avenue, Pittsburgh, PA 15213

[d] Department of Bioengineering, University of Pittsburgh, 3362 Fifth Avenue, Pittsburgh, PA 15213

ABSTRACT

As important anatomical landmarks of the human lung, accurate lobe segmentation may be useful for characterizing specific lung diseases (e.g., inflammatory, granulomatous, and neoplastic diseases). A number of investigations showed that pulmonary fissures were often incomplete in image depiction, thereby leading to the computerized identification of individual lobes a challenging task. Our purpose is to develop a fully automated algorithm for accurate identification of individual lobes regardless of the integrity of pulmonary fissures. The underlying idea of the developed lobe segmentation scheme is to use piecewise planes to approximate the detected fissures. After a rotation and a global smoothing, a number of small planes were fitted using local fissures points. The local surfaces are finally combined for lobe segmentation using a quadratic B-spline weighting strategy to assure that the segmentation is smooth. The performance of the developed scheme was assessed by comparing with a manually created reference standard on a dataset of 30 lung CT examinations. These examinations covered a number of lung diseases and were selected from a large chronic obstructive pulmonary disease (COPD) dataset. The results indicate that our scheme of lobe segmentation is efficient and accurate against incomplete fissures.

Keywords: Pulmonary lobe segmentation, piecewise fitting, b-spline fitting, computer aided diagnosis

1. Introduction

Human lungs are divided into five lobes by the lobar fissures. The left lung has two lobes (upper and lower) divided by the left oblique (major) fissure and the right lung has three lobes (upper, middle, and lower) divided by the right oblique (major) fissure or the horizontal (minor) fissure. Both bronchial and vascular systems in each lobe are largely isolated with minimal connections between lobes, and the lobes can be considered as relatively independent function units. Hence, early diseases of several types may begin in and/or be limited to an individual lobe. Accurate lobe segmentation may be useful for characterizing specific lung diseases (e.g., inflammatory, granulomatous, and neoplastic diseases) [1-2].

A number of computerized schemes aimed at identifying pulmonary lobes have been developed to date [3-16]. Existing lobe segmentation methods can be classified into two categories, namely anatomy knowledge based and shape based schemes. Anatomy knowledge based schemes depend on either local or global knowledge of the anatomy of lung structures. Considering the fact that there should not be any large vessels in the vicinity of pulmonary fissures, Kuhnigk *et al.* [3] identified lobes using an interactive 3-D watershed algorithm. To take advantage of the linear appearance of fissures, Zhou *et al.* [4*] and Saita *et al.* [5] classified the vessels and bronchi into five lobe regions using an edge detection method and the Hough transform based curved surface detection method, respectively. Zhang *et al.* [6-8] presented a method for automatic segmentation of oblique fissures using an atlas-based initialization procedure followed by a two-step graph searching procedure to delineate the fissures. The anatomy knowledge or an atlas can help to estimate the

* Email: jip13@pitt.edu

Medical Imaging 2012: Computer-Aided Diagnosis, edited by Bram van Ginneken, Carol L. Novak,
Proc. of SPIE Vol. 8315, 831535 · © 2012 SPIE · CCC code: 1605-7422/12/$18 · doi: 10.1117/12.911073

lobe margin. However, human lungs are usually different from each other, hence the accuracy of estimation based on anatomy knowledge may be limited.

More recently, researchers have became interested in two-step schemes (fissure detection and lobe segmentation). Pu *et al.* [9-10] used a computational geometry based approach, including the marching cubes algorithm (MCA), Laplacian smoothing, and extended Gaussian image (EGI), to find the fissure points and used the Radial Basis Functions (RBF) to fit the fissure points to achieve the lobe margin. Ukil *et al.* [11] used a "ridgeness" measure followed by a 3D graph search to find fissure points and used the biharmonic spline interpolation and airway landmarks to obtain the lobe margin. Rikxoort *et al.* [12-13] used second-order information to find fissure points and then used an atlas based scheme to obtain the final lobe margin. Many studies have shown that incomplete fissures are very frequent [17-18]. We need to estimate the lobe margin where fissures are incomplete. The lung fissures are usually very smooth in the 3D space, thus we can employ some interpolation/extrapolation techniques to predict the missing fissures based on existing/detected fissures. Some previous methods aimed to fit a smooth surface assisted by the second order smoothing penalty, however, the second order penalty is very sensitive to local noises (Fig. 1f).

In this study, we aim to develop a fully automated algorithm for accurate identification of individual lobes regardless of the integrity of pulmonary fissures. The underlying idea of the developed lobe segmentation scheme is to use B-spline surfaces to approximate the detected fissures. It is a hybrid of two stages of surface fitting: (1) global fissure surface smoorhing and (2) local fissure surface representation. The first one provides the coefficients of the B-spline surfaces for every fissures point. The second one is designed to fit a number of small planes using local fissures points. The local surfaces are finally combined for lobe segmentation using a quadratic B-spline weighting strategy to assure that the segmentation is smooth.

2. Method and Material

The proposed automated lobe segmentation method includes three processing stages: 1) lung volume segmentation, 2) fissure detection and classification, and 3) lobe identification. The computerized schemes used in the first two stages have been described previously[19-20]; therefore, the first two stages are briefly summarized here and the majority of this paper is focused on the lobe identification.

2.1. Lung Segmentation

In this study, we used an automated lung segmentation approach proposed in [19], namely Adaptive Border Marching Algorithm (ABMA), to segment lung volume. As a geometric technique, this algorithm is able to obtain a "smooth" lung boundary with a high computational efficiency by "bridging" regional concave regions of lung boundaries in a progressive marching manner. A detailed description of the scheme along with experimental results had been reported elsewhere [19].

2.2. Fissure Detection

After lung segmentation, a previously developed automated scheme [20] is applied to detect pulmonary fissures using a piecewise plane fitting algorithm. The underlying idea is to search for surface-like structures in the 3D Euclidean space using an efficient and robust plane fitting algorithm. The plane fitting operation is performed in a number of small spherical lung sub-volumes and is not sensitive to the presence of outliers. Using a simple clustering criterion during the detection process, the identified surfaces, assumed to represent fissures, are classified based on their spatial coherence and surface area into left oblique, right oblique and right horizontal fissures.

2.3. Lobe Segmentation

Pulmonary fissures form the boundaries between two adjacent lobes, but it is difficult to achieve a smooth segmentation of the lobes because these fissures are often incomplete, and it is extremely difficult, if not impossible, for a computerized scheme to detect all fissures depicted on CT images. When the fissure is not complete, we want to predict the missing fissure using the detected fissures. In this paper, the issue is addressed by a three step surface fitting scheme: 1) rotation, e.g., Fig 1(b); 2) smoothing using B-spline fitting assisted by first order smoothing penalty, e.g., Fig. 1(c); 3) surface fitting using piecewise plane approximation, e.g., Fig. 1(d).

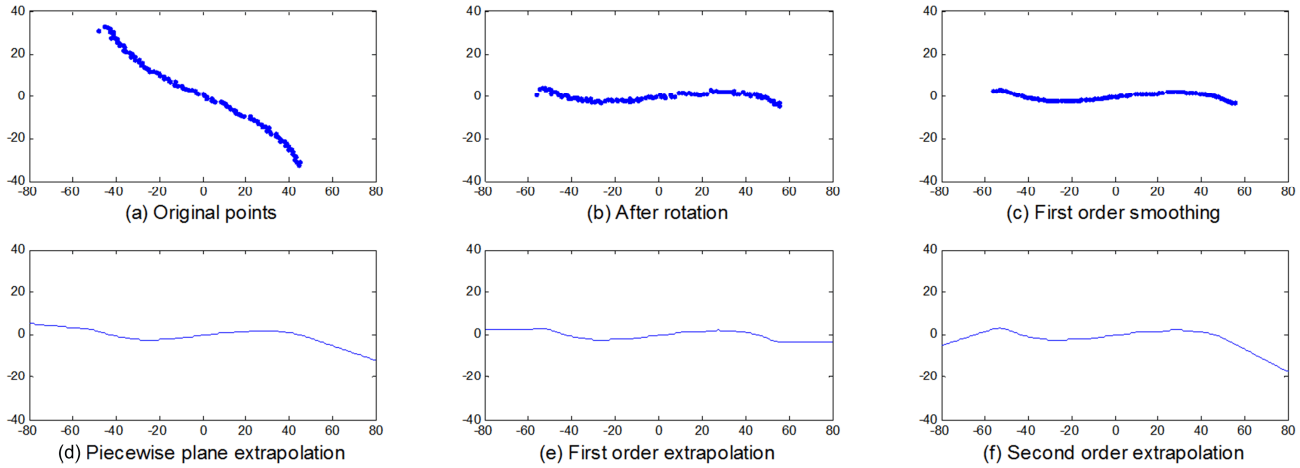

Fig 1: A two dimensional diagram of the fitting scheme. (a) the original points; (b) points after coordinate rotation; (c) points smoothing using B-spline assisted by first order smoothing penalty; (d) surface fitting and extrapolation using piecewise plane fitting; (e) surface fitting and extrapolation using B-spline fitting assisted by first order smoothing penalty; (f) surface fitting and extrapolation using B-spline fitting assisted by second order smoothing penalty.

2.3.1 Coordinate Rotation

Though the fissures are curved planes, they exists a direction for each fissure, along which the fissure looks very "flat". To utilize this information, we first rotate the coordinate (x,y,z) such that the points have minimal variance along the z axis. After rotation, we don't need to fit a stiff surface and we can include all the points in piecewise surface fitting. Let $P = \{p_i\}_{i=1}^{N}$ denote an identified fissure point set, $\lambda_1 \geq \lambda_2 \geq \lambda_3$ and $U = [u_1, u_2, u_3]$ be three eigenvalues and corresponding eigenvectors of the covariance matrix C, respectively. We transform the point set P into the new coordinate by

$$Q = U^T P = \{U^T p_i\}_{i=1}^{N} = \{q_i\}_{i=1}^{N}, \tag{1}$$

where $q_i = [x_i, y_i, z_i]^T$.

2.3.2 Global Points Smoothing

Given the rotated points $Q = \{q_i\}_{i=1}^{N}$, we then smooth the surface to reduce the noises using a quadratic B-spline fitting with the control grid size of 5×5 mm^2.

$$z = h(x, y) = \sum_{k=1}^{M} g_k(x, y) b_k \ , \tag{2}$$

where M is number of control points, b_k are coefficients and $g_k(x, y)$ are quadratic B-spline basis functions. The coefficients b_k can be solved using least square approximation. Since the B-spline fitting is used to smooth the surface points but not for extrapolation, we add a first order smoothing penalty,

$$C(h) = \int (\nabla h)^2 \, dxdy \ . \tag{3}$$

One can also add a bending energy penalty to maintain the trend, however, the bending energy is very sensitive to the margin points, as seen in Fig. 1(f). When the fissure is incomplete, the detected margin fissure points may have large noise.

Given the B-spline function, the points $Q = \{q_i\}_{i=1}^{N}$ are projected on the B-spline surface, where point $q_i = [x_i, y_i, z_i]^T$ is updated by $q_i^{new} = [x_i, y_i, h(x_i, y_i)]^T$. An example of fissure smoothing is shown in Fig. 2.

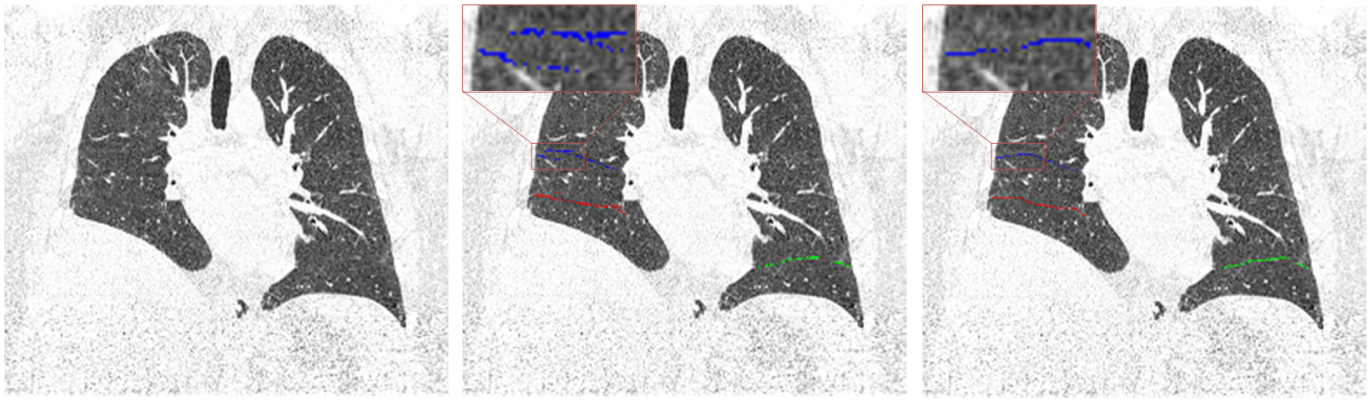

(a) Original Image (b) Detected Fissure (c) After Smoothing

Fig 2: An example of fissure smoothing.

2.3.3 Piecewise Local Surface Fitting

Centered at each control point $[x_k, y_k]$, a circle with a radius r (e.g., $r = 10$ mm) was selected. For the point set Q_k inside the circular cylinder, i.e., $Q_k = \{q_i^{new} \mid (x_i - x_k)^2 + (y_i - y_k)^2 < r^2\}$, a plane is fitted using least square fitting. In order to further reduce the effect of the margin noise, we only fit the points with area $S(Q_k)$ on the XY plane larger than $\rho\pi r^2$ (e.g., $\rho = 0.5$). Let $f_k(q) = n_k^T(q - o_k) = 0$ denote the fitted plane, where the unit vector n_k is the norm that satisfies $u_3^T n_k \geq 0$ (otherwise, we can flip the sign), and o_k is the center of the points Q_k. Then, the final fissure surface can be represented using

$$f(q) = \frac{\sum_{k=1}^{M} g'(d(q,o_k)/r) f_k(q)}{\sum_{k=1}^{M} g'(d(q,o_k)/r)} = 0 \tag{4}$$

where $d(q,o_k)$ is the Euclidean distance between point q and o_k, and $g'(t) \in C^1$ is a revised quadratic B-spline basis function,

$$g'(t) = \begin{cases} \frac{3}{4} - t^2, & t \leq \frac{1}{2} \\ \frac{1}{2}(\frac{3}{2} - t)^2, & \frac{1}{2} < t \leq 1 \\ \frac{1}{8}\exp(4 - 4t), & t > 1 \end{cases}. \tag{5}$$

We can verify that the $g'(t)$ is still once continuously differentiable and with non-zero value at all $t \geq 0 \in R$. For a point p in the original coordinate, the surface is represented by $F(p) = f(U^T p) = 0$.

2.3.4 Lobe Assignment

$F(p)$ is an implicit function with about two thousands parameters, thus it is time expensive to assign a value for each voxel inside the lung. However, for each (x, y), their exists only one z, such that $F(p) = 0$. Thus, we can use a bisection method (Fig. 3) to find the margin between two lobes.

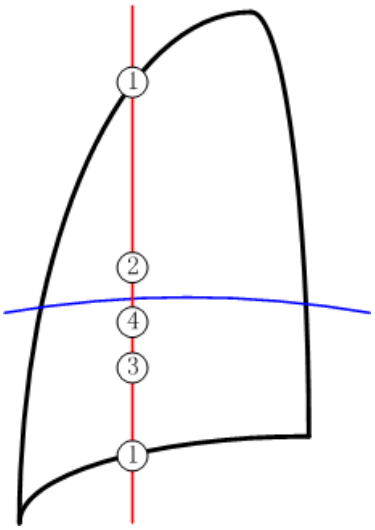

Fig. 3: A schematic diagram of the bisection method.

2.4. Performance Assessment

We assessed the performance of the proposed lobe segmentation algorithm by comparing the results obtained using the method described here with a manually created reference standard consisting of 30 CT examinations. Distance from a point p to a point set A is computed via

$$d(p, A) = \min_{q \in A} d(p, q), \tag{6}$$

where $d(p,q)$ denote the 3D Euclidean distance between points p and q. Root mean squares (RMS), mean, and maximum distances of each case between compared methods were computed.

3. Results

When creating the reference standard, a dataset of 30 lung CT examinations were selected and it covered a number of lung diseases (e.g., emphysema, ILD, PEV, pneumonia, and cystic fibrosis). Images were reconstructed using the GE Healthcare "lung" reconstruction kernel with section reconstruction interval ranged from 0.50 mm to 1.25 mm, and in-plane pixel size from 0.55 mm to 0.78 mm. A trained human image analyst manually traced the fissured depicted of these CT examinations and marked them using freehand sketches on the 2D sagittal views in a slice-by-slice manner because the sagittal view gave a relatively more straightforward concept of the types of different fissures as compared with other views (i.e., axial and coronal views). Different types of fissures were marked separately.

The discrepancies for different types of fissures from the reference standard to the results obtained by the computerized scheme were computed. The root mean squares (RMS), mean, and maximum of the discrepancies were summarized in Table 1. It can be seen that the left oblique fissures have smaller discrepancy (error) than the right oblique fissure, and the right horizontal fissures have the largest discrepancy (error). Finally, an example in Fig. 4 is used to visually demonstrate the performance of the newly developed algorithm in lobe segmentation.

Table 1: Average (±standard deviation) of RMS, mean, and maximum discrepancy (error) in Euclidean distance from the manually generated reference standard to the results obtained by the newly developed scheme on 30 CT examinations.

Fissure type	RMS (mm)	Mean (mm)	Max (mm)
left oblique fissure	1.46 ± 0.91	1.05 ± 0.48	7.00 ± 3.23
right oblique fissure	1.54 ± 0.93	1.20 ± 0.61	9.38 ± 5.40
right horizontal fissure	1.73 ± 0.94	1.36 ± 0.83	9.35 ± 5.62

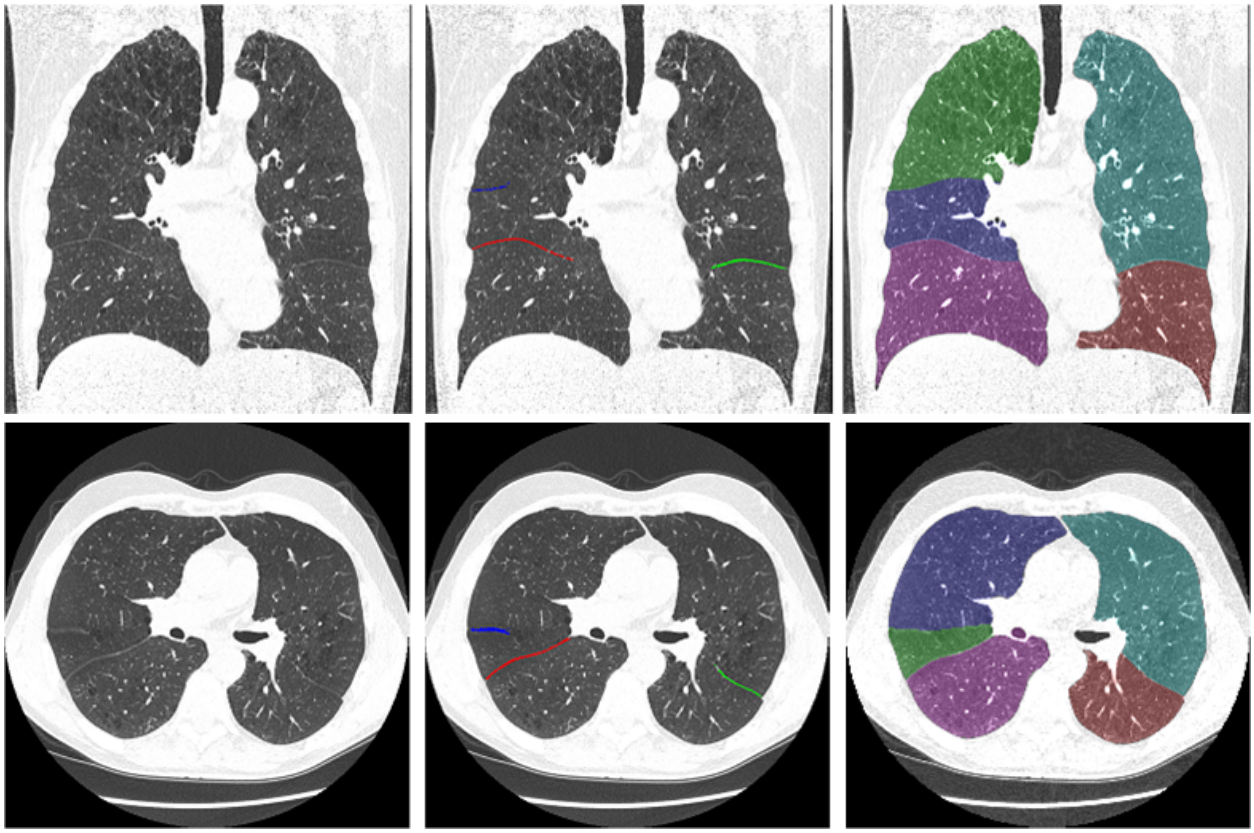

(a) Original Image (b) Fissure Detection (c) Lobe Segmentation

Fig. 4: An example demonstrating the performance of the newly developed scheme for identifying pulmonary lobes depicted with incomplete fissures. The left column shows the original CT images, the middle column shows the identified fissures in overlay, and the right column shows the identified lobes in overlay. The top and bottom rows show the coronal and axial views, respectively.

4. Discussion

The local piecewise fitting scheme is this paper is clearly different from the previous methods. Compared with the RBF surface fitting [10], the local piecewise surface fitting scheme in this paper include all the detected fissure points while the RBF fitting only use some sampled points and the scheme in this paper doesn't required additional off-surface point to assist the approximation thus we don't need to estimate the normal vector. Compared with biharmonic spline interpolation [11], our method may take advantage of the least square fitting with consideration of errors on the three directions. And the most important difference of the proposed local piecewise surface fitting from the others is that it avoids using the second order smoothing constraints to constrain the surface shape potentially reduces the noises of the detected fissures for extrapolation. An example in Fig. 5 is used to demonstrate the difference between the piecewise plane fitting algorithm (Fig. 5d) with the first order constraint (fig. 5e) or second order constraint (Fig. 5f) based extrapolation. In this case (Fig. 5), the fissures (especially the minor fissure) are incomplete (Fig. 5c). From Fig. 5d-f, we can have the same conclusion as in Fig. 1. The first order constraint based algorithm fails to extrapolate the surface accurately and the second order constraint based algorithm is sensitive to noise points.

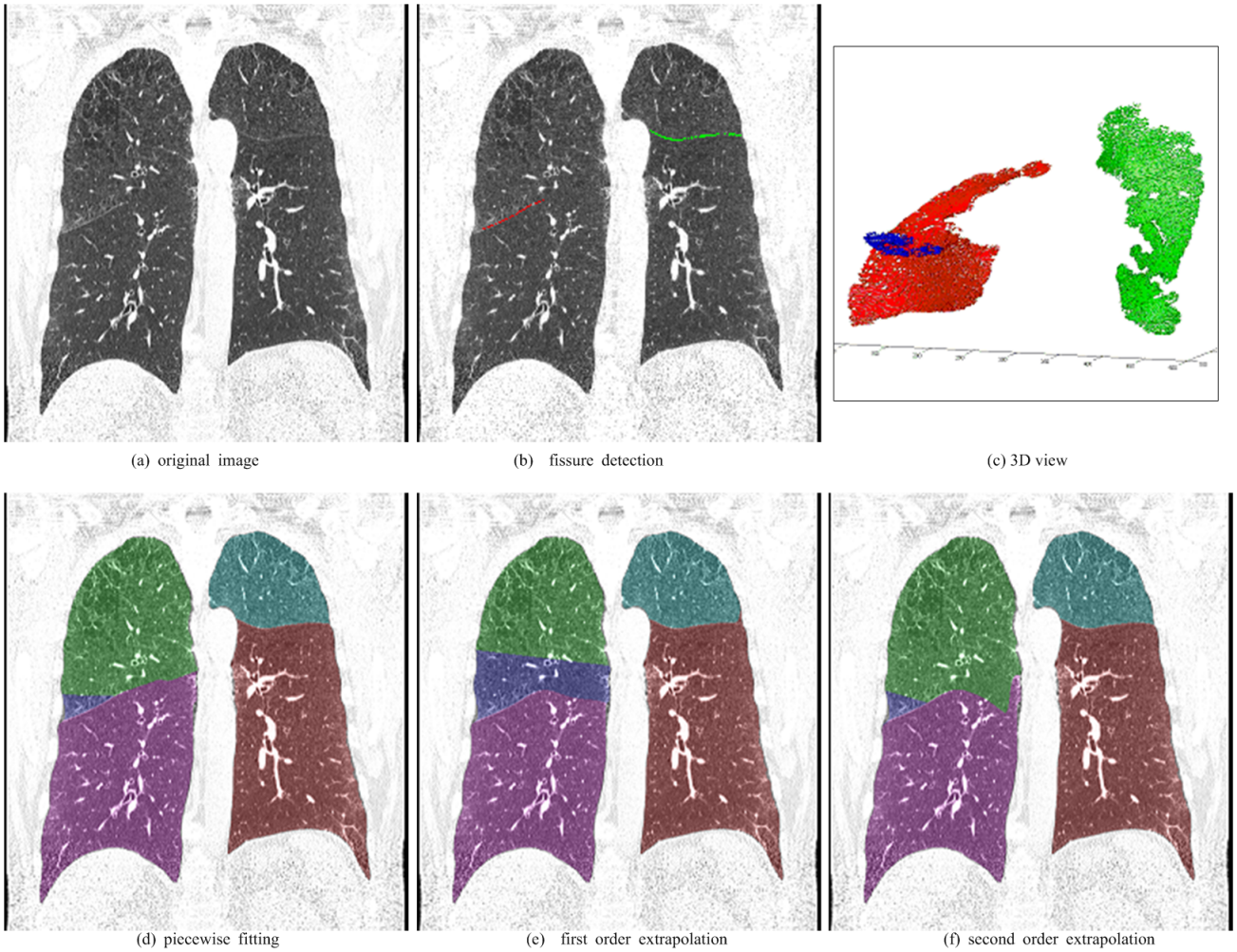

(a) original image (b) fissure detection (c) 3D view

(d) piecewise fitting (e) first order extrapolation (f) second order extrapolation

Fig. 5 Lobe identification using piecewise fitting (d), first order extrapolation (e) and second order extrapolation (f), respectively.

For a typical CT examination consisting of 300~600 image slices (with a slice thickness of), it takes approximately 2 minutes to execute our fitting scheme on a desktop PC, while the previous method [2] took approximately 25 minutes.

5. Conclusions

In this paper, a fully automatic pulmonary lobe segmentation scheme was developed. A global B-spline fitting algorithm was applied to smooth the detected fissures and a piecewise plane fitting was developed to achieve the lobe margin. Our comparison experiments with a manually created reference standard demonstrate that this newly developed scheme can achieve a reasonable performance in accuracy, robustness, and efficiency.

Acknowledge

This work was supported in part by grants R01 HL096613, P50 CA090440, P50 HL084948, and R01 HL107883, R01 HL095397, from National Institutes of Health, to the University of Pittsburgh; the SPORE in Lung Cancer Career Development Program and Bonnie J. Addario Lung Cancer Foundation.

References

[1] Modgil, V., Das, S., and Suri, R., "Anomalous lobar pattern of right lung: A case report," *Int. J. Morphol.*, vol. 24, no. 1, pp. 506–507 (2006).

[2] Venuta, F., Rendina, E. A., Giacomo, T. D., Flaishman, I., Guarino, E., Ciccone, A. M., and Ricci, C., "Technique to reduce air leaks after pulmonary lobectomy," *Eur. J. Cardio-Thoracic Surg.*, vol. 13, no. 4, pp.361–364 (1998).

[3] Kuhnigk, J. M., Hahn, H. K., Hindennach, M., Dicken, V., Krass, S. and Peitgen, H. O."Lung lobe segmentation by anatomy-guided 3d watershed transform," in *SPIE*, pp. 1482–1490 (2003).

[4] Zhou, X., Hayashi, T., Hara, T., Fujita, H., and Yokoyama, R., "Automatic recognition of lung lobes and fissures from multi-slice ct images," in *SPIE*, pp. 1629–1633 (2004).

[5] Saita, S., Kubo, M., Kawata, Y., Niki, N., Ohmatsu, H. and Moriyama, N., "An algorithm for the extraction of pulmonary fissures from low-dose multislice ct image," *System and Computers in Japan*, vol. 37, no. 9, pp. 63–76 (2006).

[6] Zhang, L. and Reinhardt J., "Detection of pulmonary lobar fissures using fuzzy logic," in *Proc. of SPIE*, pp. 188–199 (1999).

[7] Zhang, L., Hoffman, E. and Reinhardt, J. "Pulmonary lobe segmentation by graph search with 3-d shape constraints," in *SPIE*, pp. 204–215 (2001).

[8] Zhang, L., Hoffman, E. A. and Reinhardt J., "Atlas-driven lung lobe segmentation in volumetric x-ray ct images," *IEEE Transactions on Medical Imaging*, vol. 25, no. 1, pp. 1–16 (2006).

[9] Pu, J., Leader, J.K., Zheng, B., Knollmann, K., Fuhrman, C., Sciurba, F.C. and Gur, D., "A computational geometry approach to automated pulmonary fissure segmentation in ct examinations," *IEEE Transactions on Medical Imaging*, vol. 28, no. 5, pp. 710–719 (2009).

[10] Pu, J., Zheng, B., Leader, J.K., Fuhrman, C., Knollmann K., Klym, A. and Gur, D., "Pulmonary lobe segmentation in CT examinations using implicit surface fitting," *IEEE Transactions on Medical Imaging*, vol. 28, no. 12, pp. 1986–1996 (2009).

[11] Ukil, S. and Reinhardt, J. M., "Anatomy-guided lung lobe segmentation in x-ray ct images," *IEEE Transactions on Medical Imaging*, vol. 28, no. 2, pp. 202–214 (2009).

[12] E. M. van Rikxoort, B. van Ginneken, M. Klik, and M. Prokop, "Supervised enhancement filters: Application to fissure detection in chest ct scans," *IEEE Transactions on Medical Imaging*, vol. 27, no. 1, pp. 1–10, Jan. 2008.

[13] Van Rikxoort, E.M., Hoop, B., van de Vorst, S., Prokop, M. and van Ginneken, B., "Automatic segmentation of pulmonary segments from volumetric chest ct scans," *IEEE Transactions on Medical Imaging*, vol. 28, no. 4, pp. 621–630 (2009).

[14] Wang, J., Betke, M. and Ko, J., "Pulmonary fissure segmentation on CT," *Medical Image Analysis*, vol. 10, pp. 530–547 (2006).

[15] Boykov, Y. and Kolmogrov, V., "Anatomy-guided lung lobe segmentation in x-ray ct images," *IEEE Transactions on Pattern Analysis and Machine Intelligent*, vol. 26, no. 9, pp. 1124–1137 (2004).

[16] Ross, J. C., Estepar, R., Kindlman, G., dfaz, A., Westin, C.F., Silverman, E.K. and Washko, G.R.,"Automatic lung lobe segmentation using particles, thin plate splines, and maximum a posteriori estimation," *Medical Image Computing and Computer-Assisted Intervention*, pp. 163-171(2010).

[17] Pu, J., Fuhrman, C., Durick, J., Leader, J.K., Klym, A., Sciurba, F.C. and Gur, D., "Computerized Assessment of Pulmonary Fissure Integrity Using High Resolution CT," Medical Physics, Vol. 37, no. 9, pp. 4661-4672 (2010).

[18] Aziz, A., Ashizawa, K., Nagaoki, K. and Hayashi, K., "High resolution CT anatomy of the pulmonary fissures," *J. Thoracic Imag.*, vol. 19, no. 3, pp. 186–191 (2004).

[19] Pu, J., Roos, J.E., Rubin, G. D., Napel, S. and Paik, D. S., "Adaptive Border Marching Algorithm: Automatic Lung Segmentation on Chest CT Images," Computerized Medical Imaging and Graphics, Vol. 32(6): 452-462 (2008).

[20] Gu, S., Wilson, D., Siegfried, J. M., Bigbee, W.L., Gur, D. and Pu, J.,"Automated Identification of Pulmonary Fissures using a Robust Piecewise Plane Fitting Algorithm," Medical Physics, (in review) (2012).